© 2022. Published by The Company of Biologists Ltd | Journal of Cell Science (2022) 135, jcs259540. doi:10.1242/jcs.259540

RESEARCH ARTICLE

Translation initiation factor eIF4G1 modulates assembly of the polypeptide exit tunnel region in yeast ribosome biogenesis

Yun-Ting Tseng, Yu-Cheng Sung, Ching-Yu Liu and Kai-Yin Lo*

ABSTRACT

eIF4G is an important eukaryotic translation initiation factor. In this study, eIF4G1, one of the eIF4G isoforms, was shown to directly participate in biogenesis of the large (60S) ribosomal subunit in *Saccharomyces cerevisiae* cells. Mutation of eIF4G1 decreased the amount 60S ribosomal subunits significantly. The C-terminal fragment of eIF4G1 could complement the function in 60S biogenesis. Analyses of its purified complex with mass spectrometry indicated that eIF4G1 associated with the pre-60S form directly. Strong genetic and direct protein–protein interactions were observed between eIF4G1 and Ssf1 protein. Upon deletion of eIF4G1, Ssf1, Rrp15, Rrp14 and Mak16 were abnormally retained on the pre-60S complex. This purturbed the loading of Arx1 and eL31 at the polypeptide exit tunnel (PET) site and the transition to a Nog2 complex. Our data indicate that eIF4G1 is important in facilitating PET maturation and 27S processing correctly.

This article has an associated First Person interview with the first author of the paper.

KEY WORDS: Ribosome biogenesis, Translation initiation factor, Transacting factors, Brix family proteins, Polypeptide exit tunnel

INTRODUCTION

Protein synthesis is characterized by three steps: initiation, elongation and termination. Several proteins facilitate translation initiation, and these are termed initiation factors (Hershey et al., 2012; Sonenberg and Hinnebusch, 2007). The 40S ribosomal subunit is bound by eukaryotic translation initiation factors. Then, the ternary complex, consisting of eIF2-GTP and the charged initiator-methionine tRNA, is loaded to finish the assembly of the 43S pre-initiation complex. eIF4G is a scaffold protein, bridging the cap-binding protein (eIF4E) and the RNA helicase (eIF4A) bound to the mRNA. The poly(A)-binding protein (Pab1) recognizes the poly-adenylated tail of mRNA and associates with eIF4G to form a closed-loop complex (Jackson et al., 2010; Sonenberg and Hinnebusch, 2009). This mRNA and initiation factor complex associates with the 43S complex to form the 48S initiation complex, which scans the mRNA sequence to locate the AUG start codon (Gingras et al., 1999; Hentze, 1997).

Apart from its role in translation, eIF4G is also involved in the degradation of mRNAs in the nucleus (Das et al., 2014). The degradation of nuclear RNA primarily depends on nuclear RNA exosome-mediated decay and degradation of mRNA in the nucleus (the latter of which is termed DRN). DRN is dependent on the nuclear cap-binding complex and nuclear exosomes. eIF4G has been shown to associate with nuclear cap-binding proteins in the nucleus in humans (McKendrick et al., 2001) and yeast (Das et al., 2014) and be involved in DRN. In addition, yeast eIF4G interacts with protein components of the splicing machinery involved in pre-mRNA processing events (Kafasla et al., 2009).

Moreover, a decrease of the 60S subunit in the eIF4G1 mutant yeast strain suggests that eIF4G1 might play a role, directly or indirectly, in 60S ribosome biogenesis (Li et al., 2009). Ribosomes are responsible for protein synthesis, and their structures are highly conserved in bacteria, archaea and eukaryotes. The ribosome and its biogenesis are tightly linked to development in all kingdoms of life. Impaired ribosome assembly leads to a deficiency in translational capacity and accuracy, causing growth retardation or death in single cells, including bacteria and yeast. In higher eukaryotic organisms, such as mammals and plants, ribosome synthesis defects result in embryonic lethality and developmental defects (Wang et al., 2015; Weis et al., 2015).

Ribosomes contain both ribosomal proteins and rRNAs. More than 200 transacting factors that act in the assembly process have been discovered. The 35S rRNA is transcribed by RNA polymerase I. Cleavage at the A2 site within internal transcribed spacer 1 (ITS1) separates the 35S rRNA into the 20S and 27S rRNAs, which are the precursors of 18S and 5.8S/25S rRNAs, respectively (Baßler and Hurt, 2019; Gerhardy et al., 2014; Klinge and Woolford, 2019; Konikkat and Woolford, 2017; Kressler et al., 2017; Panse and Johnson, 2010; Peña et al., 2017; Woolford and Baserga, 2013). The 25S rRNA in the large (60S) subunit consists of six conserved domains (I to VI). Cryo-electron microscopy (EM) structures of pre-60S subunits have revealed that assembly factors assist the folding of these domains at the nucleolar stage (Kater et al., 2017; Sanghai et al., 2018; Zhou et al., 2019). Mak16, Rpf1, Nsa1, Rrp1, Ssf1, Rrp15, Rrp14, Brx1 and Ebp2 form a ring around the center of the state 2/B particle (containing 27SB rRNA), bridging the interactions between 25S rRNA domains I, II and VI. The release of these factors enables downstream maturation events. For example, the removal of Ssf1 and Rrp15 allows the subsequent loading of eL31 (formerly called Rpl31; Ban et al., 2014) around the polypeptide exit tunnel (PET) site (Sanghai et al., 2018). The release of Rpf1, Mak16, Rrp1 and Nsa1 enable the formation of the outer portion of the PET during the transition from state C to state E. The exit of Ebp2, Brx1, Noc3, Spb1, Nop2 and Nip7 allows the formation of the Nog2 particle (containing 27SB and the 25.5S+7S rRNA), and enables the formation of a functional PET (Kater et al., 2017; Sanghai et al., 2018; Zhou et al., 2019). The 5S rRNA is transcribed separately by RNA polymerase III. It co-assembles with uL18 (formerly called Rpl5; Ban et al., 2014), uL5 (formerly called Rpl11), Rpf2 and Rrs1 to associate with the early pre-60S subunits (Zhang et al., 2007). It forms the central

Department of Agricultural Chemistry, College of Bioresources and Agriculture, National Taiwan University, Taipei 10617, Taiwan.

*Author for correspondence (kaiyin@ntu.edu.tw)

K.-Y.L., 0000-0003-0440-6836

Handling Editor: Maria Carmo-Fonseca
Received 1 November 2021; Accepted 12 May 2022

Journal of Cell Science (2022) 135, jcs259540. doi:10.1242/jcs.259540

protuberance, which is required for the assembly of the Nog2 complex (Talkish et al., 2012). eIF4G2 has been shown to have genetic interaction with Ssf1, Brx1, Rpf1 and Rpf2 at the assembly stages described above (Bogengruber et al., 2003). However, its functional role is still not clear.

In this study, we characterized the functional role of eIF4G1 in ribosome synthesis and elucidated the molecular mechanisms of its action. We found that eIF4G1 directly interacted with 'biogenesis of ribosomes in *Xenopus*' (Brix) family proteins and showed strong genetic interaction with *SSF1* and its paralog *SSF2*. In *eIF4G1*Δ cells, Ssf1 and its associated factors, Rrp15, Rrp14 and Mak16, were not correctly released from the pre-60S complex. This event affected the loading of Arx1 and eL31 at the PET site and the transition to the Nog2 complex. Taken together, these data suggest that eIF4G1 is a novel trans-acting factor in 60S ribosome biogenesis.

RESULTS

eIF4G1 functions directly in 60S ribosome biogenesis

In budding yeast, there are two paralogs of eIF4G, eIF4G1 and eIF4G2, encoded by *TIF4631* and *TIF4632*, respectively (Goyer et al., 1993). Their amino acid sequences are 51% identical (72% similar) and more conserved at the C-terminus (Clarkson et al., 2010). eIF4G1 is expressed at a higher abundance than eIF4G2 (Clarkson et al., 2010). Although simultaneous deletion causes lethality (Goyer et al., 1993), deletion of eIF4G1, but not eIF4G2, impairs cellular growth (Fig. 1A). Mutants that disrupt ribosome biogenesis usually show cold-sensitive growth defects. Indeed, the growth defect of *tif4631*Δ at 20°C was more severe than at 30°C, the optimal yeast growth temperature (Fig. 1A).

We analyzed polysome profiles by sucrose gradient sedimentation of extracts from the *tif4631*Δ or *tif4632*Δ strain. Consistent with the above results, deletion of *TIF4631* led to a more dramatic defect in translation and the free 60S subunit level, whereas the defect in *tif4632*Δ was much more subtle (Fig. 1B, lower polysome and 60S peaks in *tif4631*Δ compared with those in *tif4632*Δ). The calculated free 60S to 40S ratio of wild-type (WT) cells was normalized to 1, and this ratio decreased to 0.3 and 0.7 in *tif4631*Δ and *tif4632*Δ cells, respectively (Fig. 1B). The levels of total 60S and 40S subunits were further examined under conditions that caused dissociation of subunits. The amounts of both subunits decreased in *tif4631*Δ, but the 60S exhibited a more significant decrease relative to 40S (Fig. 1C). Quantification of peaks yielded a 60S-to-40S ratio of 1.9 for the WT and 1.5 for the *tif4631*Δ mutant (Fig. 1C). Thus, these data indicate that there is a reduction of 60S subunits in the *tif4631*Δ mutant.

We also monitored the 40S and 60S subunit export in these strains. uL23–GFP was distributed normally at 30°C. Nuclear retention of uL23–GFP was observed in *tif4631*Δ cells at low temperature (Fig. 1D). Another reporter for 60S subunits, uL5–GFP, was also accumulated in the nucleus in *tif4631*Δ cells at low temperature (Fig. S1A). In contrast, uS5–GFP showed a normal cytoplasmic distribution in WT, *tif4631*Δ, and *tif4632*Δ cells even at low temperature, indicating no export defect of the 40S subunit (Fig. S1A).

The localizations (Fig. S1B) and levels (Fig. S1C) of the 60S and 40S were checked in *tif1*Δ or *tif3*Δ mutants with deletion of another translation initiation factor, eIF4A or eIF4B, respectively, to compare with the results seen upon eIF4G deletion. However, no alterations were observed. Therefore, the defects in 60S subunits were not from global perturbations of translation but the absence of eIF4G1 function in 60S biogenesis.

Northern blotting was also used to analyze the pre-rRNA intermediates in WT, *tif4631*Δ and *tif4632*Δ strains by using probes indicated on the pre-rRNA processing pathway (Fig. 1E). The levels of 35S and 27SA2 pre-rRNAs were significantly increased, and those for 23S and 20S were slightly increased in *tif4631*Δ and *tif4632*Δ mutants, supporting the observation that the defects in 60S synthesis were more severe than those in 40S synthesis. In both cases, *tif4631*Δ cells showed more abnormal accumulations of pre-rRNAs (Fig. 1E).

To determine whether eIF4G1 was directly involved in the pre-60S assembly pathway, eIF4G1 was expressed with a glutathione transferase (GST) tag and purified with glutathione beads. The proteins associated with GST alone and GST–eIF4G1 were analyzed with mass spectrometry. The enrichment of proteins calculated against GST control is shown in the volcano plot (Fig. 1F). Many 60S ribosome assembly factors, especially those at the nucleolar stage, were enriched with eIF4G1. Several biogenesis factors with a TAP tag were used to purify pre-60S complexes to further demonstrate this interaction. eIF4G1 could be detected on pre-60S ribosomal subunits (Fig. 1G).

The C-terminal fragment of eIF4G1 was important for function in 60S biogenesis

The structure of eIF4G1 has not yet been solved. Several important domains have been identified within eIF4G1, including the poly-A binding protein (Pab1), 4E and 4A (MIF4G) domains, which interact with Pab1, eIF4E and eIF4A, respectively (Fig. 2A) (Altmann et al., 1997; Clarkson et al., 2010; Dominguez et al., 1999; Tarun and Sachs, 1996). Several eIF4G1 truncation mutants were created to determine which domain was critical for its function in 60S ribosome biogenesis. The protein levels of each mutant were similar, but eIF4G1(NfΔ4E) and eIF4G1(Cf) had slightly higher expression (Fig. S2A). Whereas eIF4G1(NfΔ4E), eIF4G1(Δ4E) and eIF4G1(Δ4A) lost the ability to complement the growth of *tif4631*Δ cells, eIF4G1(ΔPab1)- and eIF4G1(Cf)-expressing *tif4631*Δ cells maintained similar growth rates to the WT. Further removal of the 4E domain from the C-terminal fragment [eIF4G1(CfΔ4E)] also meant the ability to complement growth was lost (Fig. 2B).

To correlate the growth patterns of eIF4G1 mutants with its function in 60S biogenesis, the polysome profiles (Fig. 2C) and the localization of 60S subunits (Fig. S2B) were analyzed. Consistent with the above results, *tif4631*Δ cells expressing eIF4G1(ΔPab1) did not show defects in 60S ribosome biogenesis, suggesting that deletion of the Pab1 domain does not affect ribosome biogenesis (Fig. 2C). 60S subunits were decreased and concentrated in the nucleus in eIF4G1(Δ4E) and eIF4G1(Δ4A) mutants (Fig. 2C; Fig. S2B). Notably, expression of the C-terminal fragment [eIF4G1(Cf)] maintained levels of 60S ribosome biogenesis, and its association across sucrose gradients was more concentrated at the 60S (frac. 5) and 80S (frac. 7) fractions. eIF4G1(CfΔ4E), with a deletion of the 4E domain from the C-terminal fragment, still maintained the interaction with the ribosome and was even more concentrated at the 60S (frac. 5 and 6), but the 60S ribosome level was decreased. Although deletion of the 4A domain [eIF4G1(Δ4A)] partially disrupted the eIF4G1 association with the ribosome (Fig. 2C), the N-terminal fragment [eIF4G1(NfΔ4E)], with the complete removal of the C-terminus, lost the ability to interact with ribosomes and the ability to support the synthesis of 60S subunits (Fig. 2C; Fig. S2B). The cellular distributions of these mutants were further examined. eIF4G1 was mainly distributed in the cytoplasm (Fig. 2D) and could be detected in the nucleus under overexpression (Fig. S2C). All the other mutants were distributed throughout

Journal of Cell Science (2022) 135, jcs259540. doi:10.1242/jcs.259540

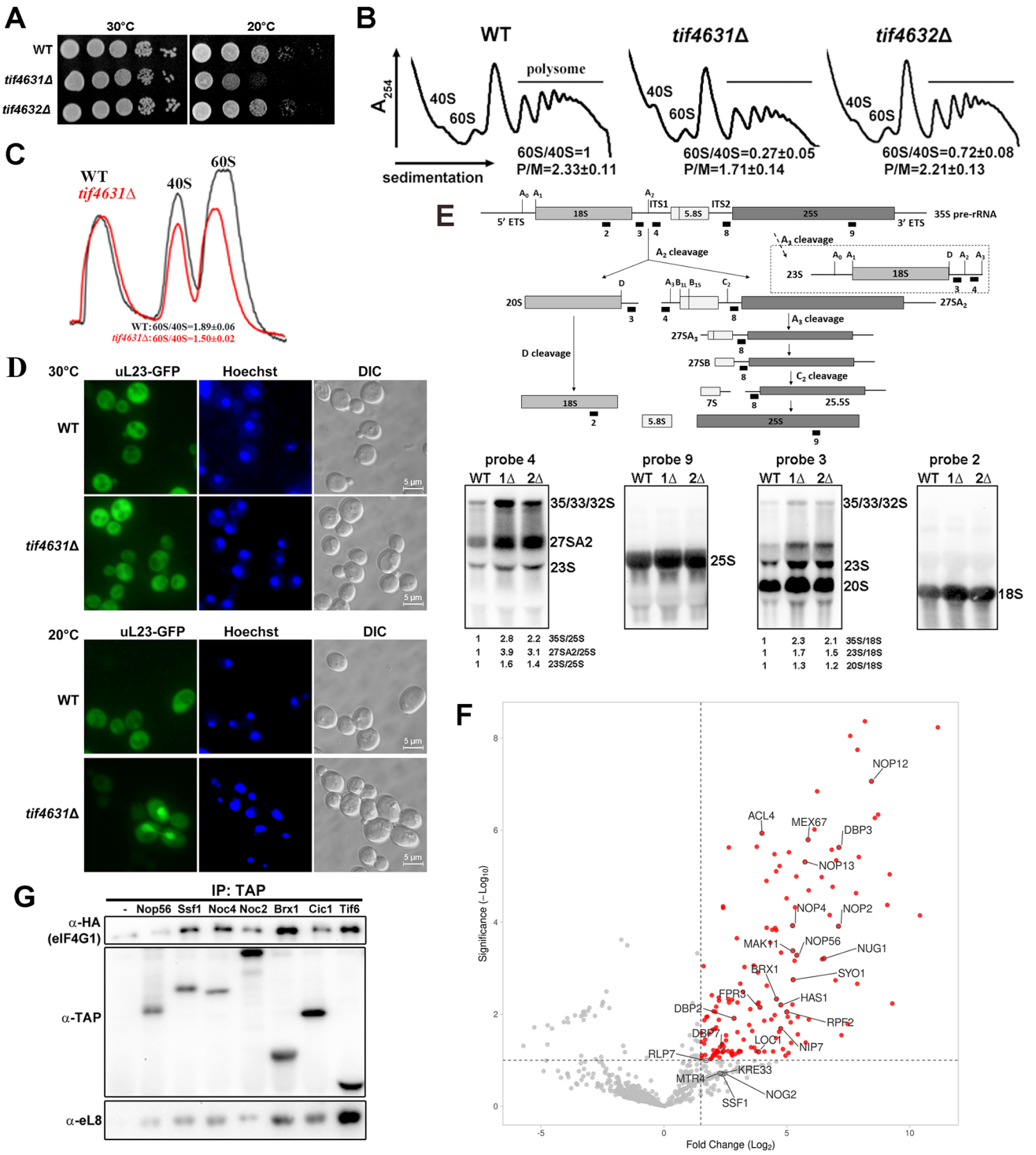

Fig. 1. eIF4G1 has a functional connection with 60S biogenesis. (A) Growth test of WT, *tif4631Δ* and *tif4632Δ* cells. (B) WT, *tif4631Δ* and *tif4632Δ* cells were cultured at 30°C, and the polysome profiles were analyzed. The calculated 60S to 40S ratio (60/40) and polysome to monosome ratio (P/M) were shown. All experiments were performed in replicates independently, and representative images are shown (results beneath are mean±s.d., *n*=2). (C) The monosome profiles were analyzed in WT and *tif4631Δ*. The ratio between the 40S and 60S subunits was calculated based on two independent experiments (mean±s.d., *n*=2). (D) The localizations of 60S (uL23–GFP) were monitored in the WT and *tif4631Δ* strains at 30°C and 20°C. (E) Detection of rRNA processing with northern blotting. The probes used in this study were indicated on the diagram, and the sequences are listed in Table S3. Values underneath the blots are the ratio between the pre-rRNA and mature RNA for the blots shown. Δ1, *tif4631Δ*; Δ2, *tif4632Δ*. (F) Proteins associated with GST alone and GST–eIF4G1 were quantified with mass spectrometry, and the relative ratio (GST–eIF4G1/GST) was calculated from two independent experiments. The proteins that were enriched more than 2-fold and had a significance [$-\log_{10}$(*P*-value)] of more than 1 are labeled in red. Ribosome biogenesis factors are labeled. (G) pre-60S subunits were purified (immunoprecipitated; IP) with IgG beads from various TAP-tagged strains. The signals were detected with western blotting. Images in A, D, E and G are representative of two experiments.

Journal of Cell Science (2022) 135, jcs259540. doi:10.1242/jcs.259540

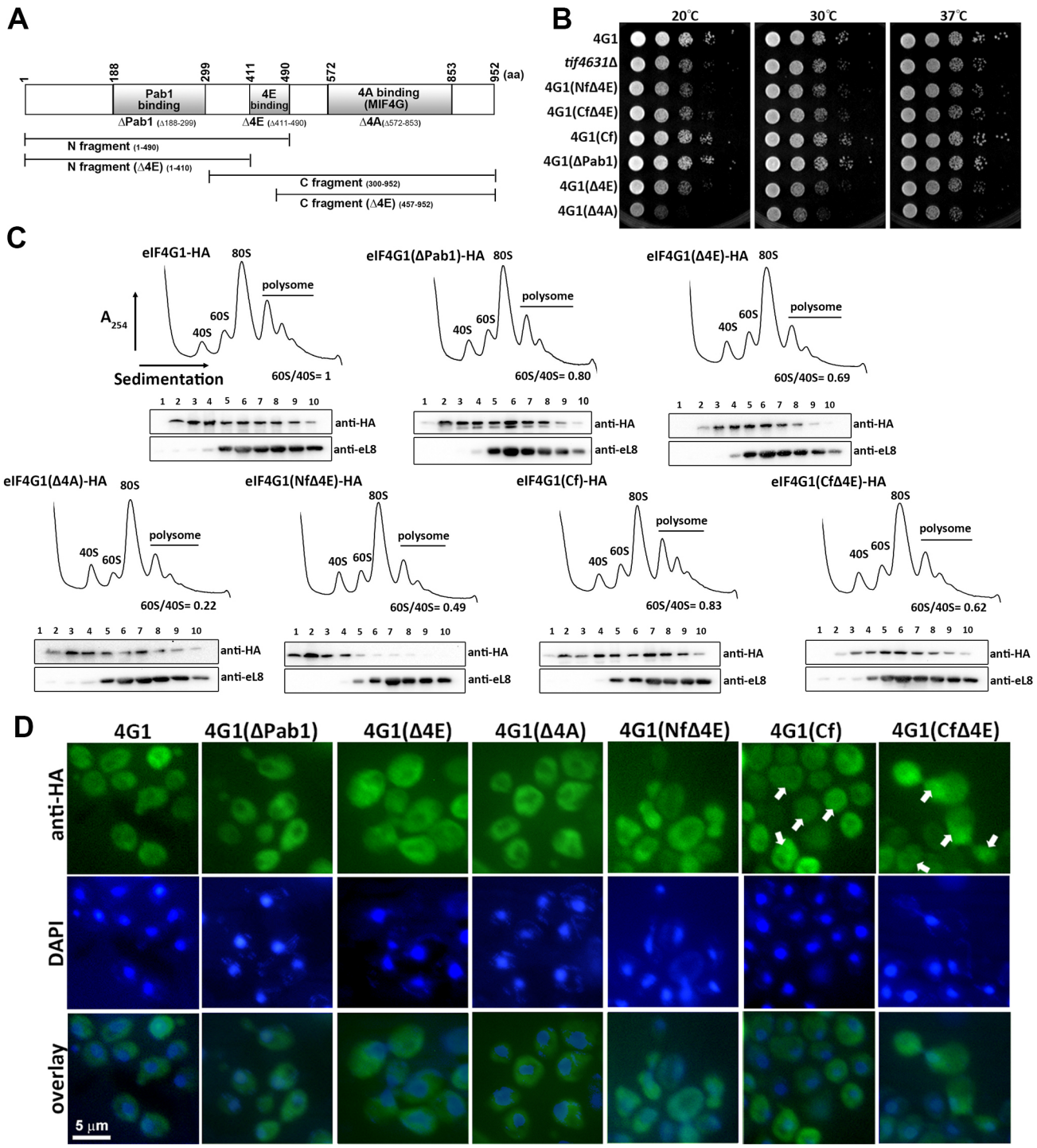

Fig. 2. The C-terminus of eIF4G1 was critical for interaction and function in 60S biogenesis. (A) Diagram of various functional domains of yeast eIF4G1 and the constructs of different eIF4G1 mutants used in this study; fragment is denoted 'f' in the construct names. (B) Growth test of *tif4631*Δ cells expressing WT (4G1 row) and various eIF4G1 mutants at different temperatures. (C) Cell lysates from different eIF4G1 mutants were fractionated in a 7–47% sucrose gradient. The polysome profiles and the distributions of each protein across the gradient were detected. (D) The cellular distributions of eIF4G1 and each eIF4G1 mutant were detected by immunofluorescence with anti-HA antibody and FITC goat-anti-mouse-IgG Ab. The position of the nucleus is indicated with a white arrow. Scale bar: 5 μm. All images are representative of two experiments.

the cytoplasm, with eIF4G1(Cf) also slightly accumulated in the nucleus. Further deletion of the 4E-binding domain enhanced the nuclear accumulation [eIF4G1(CfΔ4E); Fig. 2D; Fig. S2D).

These data suggest that the C-terminal fragment of eIF4G1, including the 4E and 4A domains, can support its association with 60S subunits and function in ribosome biogenesis. Although the 4E domain was not required for interaction with the 60S, it was required to generate normal 60S levels in cells.

eIF4G1 mutation impairs the assembly of pre-60S subunits

The eIF4G1-containing complex was immunoprecipitated, and the associated pre-rRNAs were analyzed by northern blotting to analyze

Journal of Cell Science (2022) 135, jcs259540. doi:10.1242/jcs.259540

at which stage eIF4G1 joined. eIF4G1(CfΔ4E) was also included because it showed a stronger association with pre-ribosome and nuclear retention (Fig. 2). Both eIF4G1 and eIF4G1(CfΔ4E) were predominantly associated with 27S rRNA (Fig. 3A), whereas eIF4G1(CfΔ4E) exhibited a stronger signal, consistent with its stronger association with the pre-ribosome in the results above (Fig. 2). Together with the mass spectrometry data above (Fig. 1F), these results suggest that eIF4G1 might join during the nucleolar to nuclear 60S assembly stage.

To analyze how the absence of eIF4G1 changed the ribosome biogenesis pathway, Nsa1–TAP and Rlp7–TAP (Fig. 3B) were chosen to purify the pre-60S ribosomal subunits from WT and *tif4631*Δ cells. Nsa1 can pull down early to state E (27SB) ribosomes before C2 cleavage, and Rlp7 can purify particles before Nog2 complex formation (27SB, 25.5S+7S), whose ITS2 has been processed at C2 (Braun et al., 2020; Klinge and Woolford, 2019; Sanghai et al., 2018) (Fig. 3B). Thus, a comparison of these two complexes could identify the differences in protein components before and after the release of Nsa1.

Semi-quantitative mass spectrometry analyses were performed to analyze these isolated complexes (Fig. 3C). The relative abundances of proteins were calculated between WT and *tif4631*Δ cells from three independent experiments. Only the fold differences greater than two and smaller than 0.5 were considered significant. In *tif4631*Δ cells, the levels of many factors that should have been released after state 2/B, including Ssf1, Rrp15, Rrp14, Mak11, Rpf1 and Mak16, and after state E, including Has1, Ytm1, Erb1, Nop2 and Nip7, were increased (Fig. 3B,C), whereas the levels of factors

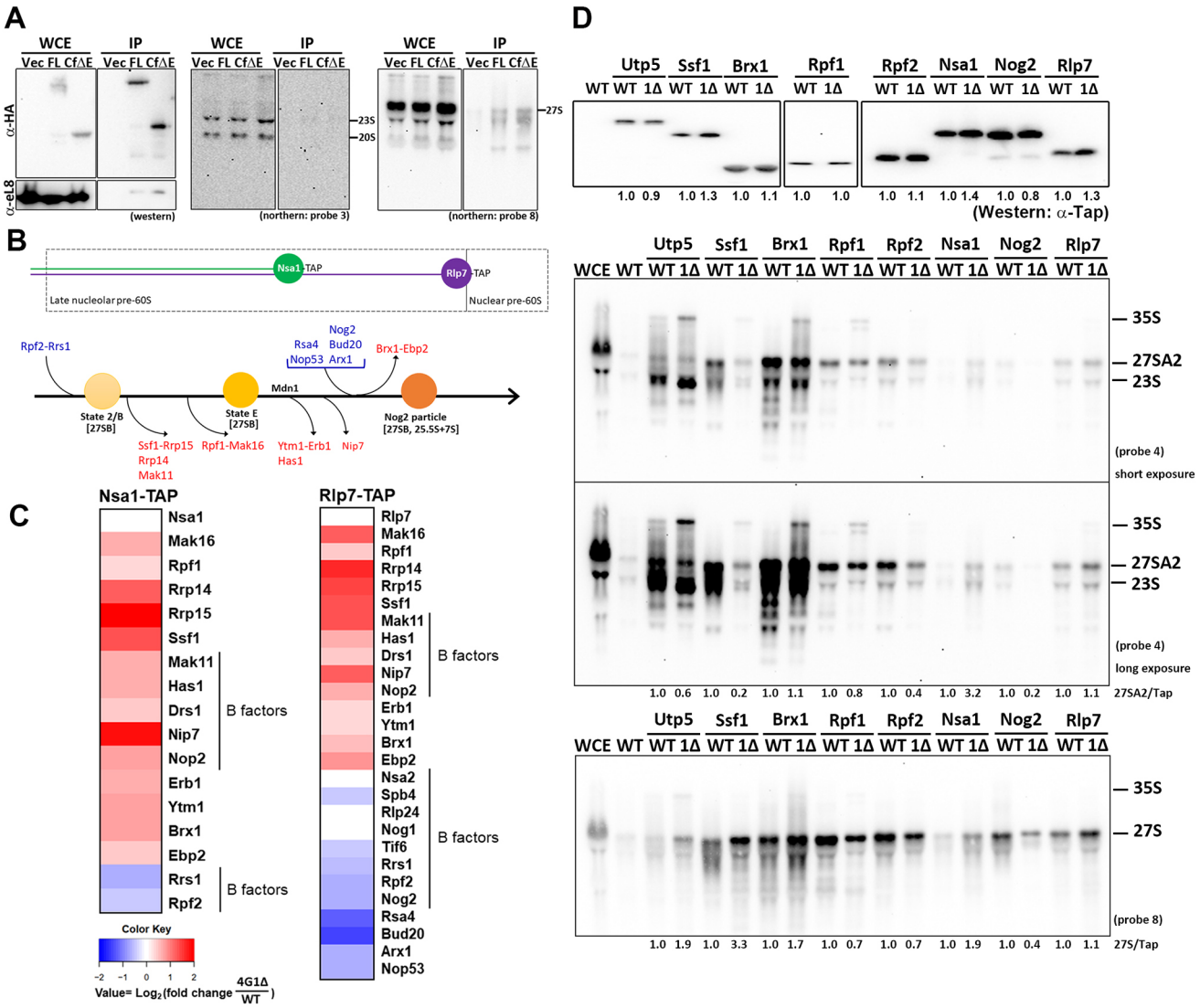

Fig. 3. The *tif4631*Δ mutant affected 60S biogenesis majorly at the 27S processing stage. (A) eIF4G1–HA (FL) and eIF4G1(CfΔ4E)–HA (CfΔE) from *tif4631*Δ cells were immunoprecipitated (IP) with anti-HA antibodies. The associated pre-rRNAs were analyzed with northern blotting using the indicated probes; a western blot for eL8 and HA is also shown. WCE, whole-cell extract; Vec, vector only. (B) The loading of the assembly factors for pre-60S subunits is depicted. The factors increased and decreased in the mass spectrometry analysis are labeled with red and blue, respectively. (C) Heatmap of assembly factors identified in the semi-quantitative mass spectroscopy analysis of the Nsa1- and Rlp7-associated ribosomal complex. The relative abundances were calculated between WT and *tif4631*Δ from three independent experiments. The color indicates the log2 of this relative ratio. (D) Pre-60S ribosomal subunits were purified with TAP-tagged assembly factors from WT and *tif4631*Δ (Δ1) cells. The TAP signals were detected by western blotting (top). The associated pre-rRNAs were separated in formaldehyde agarose gel and analyzed with northern blotting using the indicated probes. The ratio between the pre-rRNA and TAP signal for the blots shown in the figure is presented. Images in A and D are representative of two experiments.

Journal of Cell Science (2022) 135, jcs259540. doi:10.1242/jcs.259540

that should have been loaded after state E, including Nop53, Nog2, Arx1, Bud20, and Rsa4, were decreased (Fig. 3B,C). Rsa4 interacts with Mdn1, which is essential for the ATP-dependent dissociation of many assembly factors. Mdn1 releases Erb1 and Ytm1 to expose the Nop53-binding site. Nop53 then subsequently facilitates the release of Nop16 and Has1 (Sanghai et al., 2018). Arx1 (Bradatsch et al., 2007; Hung et al., 2008) and Bud20 (Baßler et al., 2012) are required for 60S ribosome export (Fig. 3B). Nog2 is the last factor loaded onto the pre-60S complex before the cleavage of 27S rRNA at the C2 site. Its recruitment depends on the proper loading of the B factors (indicated in Fig. 3C; Talkish et al., 2012). The levels of several proteins were also checked by western blotting, and the changes were consistent with the trend in mass analysis (Fig. S2E). These data imply that the primary blockage in *tif4631*Δ cells might be at the 27SB stage transition to Nog2 particle complexes.

To further examine the alterations of pre-60S ribosomes affected by the loss of eIF4G1, the associated rRNAs in affinity-purified particles at different maturation stages were analyzed (Fig. 3D). Utp5 is a component involved in 90S pre-ribosome assembly, and its associated 35S and 23S rRNAs were increased in *tif4631*Δ cells. Among the Brix family proteins, Ssf1 showed the most significant changes. Ssf1-associated rRNAs showed a 5-fold decrease of 27SA2 and a 3-fold increase of 27S species in *tif4631*Δ cells; Brx1-, Rpf1- and Rpf2-associated rRNAs showed slight alterations of 27S. Enhanced 35S rRNA signals could be detected for the Ssf1-, Brx1- and Rpf1-containing pre-60S in *tif4631*Δ, indicating either the association with 90S-like particles or that the 35S rRNA was improperly processed at these stages. Nog2 associated with significantly lower rRNA amounts, likely resulting from its decreased association with the pre-60S in *tif4631*Δ (Fig. 3D). This is consistent with the mass spectrometry result (Fig. 3C). The data above indicate that loss of eIF4G1 impaired correct associations of ribosome assembly factors and resulted in abnormal cleavages of rRNAs.

*tif4631*Δ shows strong synthetic growth defects with *ssf1*Δ and *ssf2*Δ mutants

From the data above, Ssf1, Rrp15, Rrp14 and Mak16 were accumulated in the Nsa1 and Rlp7 complexes (Fig. 3C), and the rRNA contents of Ssf1 complex altered the most in *tif4631*Δ (Fig. 3D). On the pre-60S, these proteins are localized in proximity to the peptide exit tunnel (PET) (Fig. 4A). Yeast has six Brix family proteins, Ssf1 and Ssf2, Rpf1, Brx1, Rpf2 and Imp4 (Fig. 4B), and each has its binding partner Rrp15, Mak16, Ebp2, Rrs1 and Mpp10, respectively, interacting at the Brix domain (Zhou et al., 2019). Excepting Imp4, which is involved in 40S ribosome biogenesis (Lee and Baserga, 1999), the rest of these Brix family proteins are all involved in 60S ribosome biogenesis (Fatica et al., 2002; Kaser et al., 2001; Wehner and Baserga, 2002). Rpf2 and Rrs1 are required to recruit 5S rRNP onto nascent ribosomes (Asano et al., 2015; Calviño et al., 2015; Kharde et al., 2015; Madru et al., 2015; Zhang et al., 2007). Ssf1, Rpf1 and Brx1 are present at similar stages in the early nucleolar pre-60S ribosome (Fig. 3B) (Sanghai et al., 2018; Zhou et al., 2019), and they accumulated abnormally in *tif4631*Δ (Fig. 3C).

Genetic interactions were examined using double mutants to explore the potential connections between eIF4G and Brix family proteins (Fig. 4C; Fig. S3A–C). *SSF1* and *SSF2* are paralogs, with 94% identical amino acid sequences (Yu and Hirsch, 1995). Although *ssf1*Δ cells showed a slight growth defect, and *ssf2*Δ cells showed a WT growth rate at 20°C, 30°C and 37°C, after combination with *tif4631*Δ or *tif4632*Δ, *tif4631*Δ*ssf1*Δ, *tif4632*Δ*ssf1*Δ and *tif4631*Δ*ssf2*Δ showed strong synthetic growth defects (Fig. 4C). *tet-BRX1* (Fig. S3A), *GAL::RPF1* (Fig. S3B) and *GAL::RPF2* (Fig. S3C) were also crossed with *tif4631*Δ or *tif4632*Δ. In the absence of doxycycline, *tif4631*Δ*tet-BRX1* demonstrated a slower growth rate. The addition of doxycycline exacerbated the growth (Fig. S3A). Similarly, the double mutants created between *GAL::RPF1* or *GAL::RPF2* and *tif4631*Δ or *tif4632*Δ also exhibited slower growth when the galactose-driven promoter was partially repressed by culture in medium containing 1% galactose and 1% glucose (Fig. S3C). However, the enhancements of synthetic growth defects with *tif4631*Δ were not as dramatic as for the *ssf1*Δ or *ssf2*Δ mutant.

eIF4G1 directly interacts with Brix family proteins

The structures of Ssf1, Brx1, Rpf1 (Kater et al., 2017; Sanghai et al., 2018; Zhou et al., 2019) and Rpf2 (Madru et al., 2015; Schuller et al., 2018; Sun et al., 2017; Wu et al., 2016) have been previously solved. The structures of these four proteins were compared. Apart from the Brix domain, Brx1, Rpf1 and Rpf2 have an extra helix at the N- or C-terminus (Fig. 4D). The N-terminal 22 amino acids and the C-terminal 97 amino acids (from V357 to E453) of Ssf1 have not been solved on the structure (PDB 6C0F; Sanghai et al., 2018). The C-terminus might also form a long helix based on secondary structure prediction (CFSSP server) (Kumar, 2013).

We next analyzed whether eIF4G1 interacted directly with Brix family proteins (Fig. 4E,F). Recombinant eIF4G1 was overexpressed in *Escherichia coli* with a GST tag. Ssf1, Brx1, Rpf1 or Rpf2 was overexpressed with His_6 tags. Whereas free GST pulldown did not bring any Brix family proteins, GST–eIF4G1 could pull down Ssf1, Brx1, Rpf1 and Rpf2 (Fig. S3D). Our above results have demonstrated that the C-terminus of eIF4G1 is important for ribosome association (Fig. 2C). Thus, eIF4G1(Cf) and eIF4G1(CfΔE) were expressed and examined the interaction. These two C-terminal constructs also directly interacted with Ssf1, Brx1, Rpf1 and Rpf2 (Fig. 4E,F). To determine whether the core Brix domain is necessary for eIF4G1 binding, we removed the 111 amino acids (from E343 to E453) from the C-terminus of Ssf1 (Fig. 4B) and expressed the Brix domain only. Both eIF4G1(Cf) and eIF4G1(CfΔE) maintained a similar interaction with the Brix domain of Ssf1 (Fig. 4E, ssf1ΔC). Therefore, eIF4G1 presumably uses the C-terminus to interact with pre-60S via the Brix protein(s).

eIF4G1 mutation caused retention of Ssf1 and blocked the loading of eL31 and Arx1

Since *tif4631*Δ showed genetic and physical interaction with Brix family proteins, the protein levels and stability of Ssf1, Brx1, Rpf1 and Rpf2 were examined in *tif4631*Δ cells. However, there were no changes in protein stability (Fig. S3E). Therefore, eIF4G1 is not required to maintain the levels of Brix family proteins.

The mass spectrometry data (Fig. 3B,C) suggested that some assembly factors, including Ssf1, could show abnormal retention on the pre-60S. Ssf1 association with pre-60S was therefore examined in *tif4631*Δ and *tif4632*Δ cells by western blotting to test this possibility. Puf6 was used to purify nucleolar ribosomal subunits (Qiu et al., 2014; Yang et al., 2016). Tif6 is loaded in the nucleolus and released at a late 60S maturation step in the cytoplasm (Lo et al., 2010). Ssf1 was highly enriched in *tif4631*Δ cells and slightly increased in *tif4632*Δ cells (Fig. 5A). The cellular localization of Ssf1, Brx1, Rpf1 and Rpf2 was also examined in the cells. To avoid potential interference from its paralog, the localization of Ssf1–GFP was observed in *ssf2*Δ cells. We found that Ssf1 was partially mislocalized from the nucleolus to the nucleoplasm in *tif4631*Δ and

Journal of Cell Science (2022) 135, jcs259540. doi:10.1242/jcs.259540

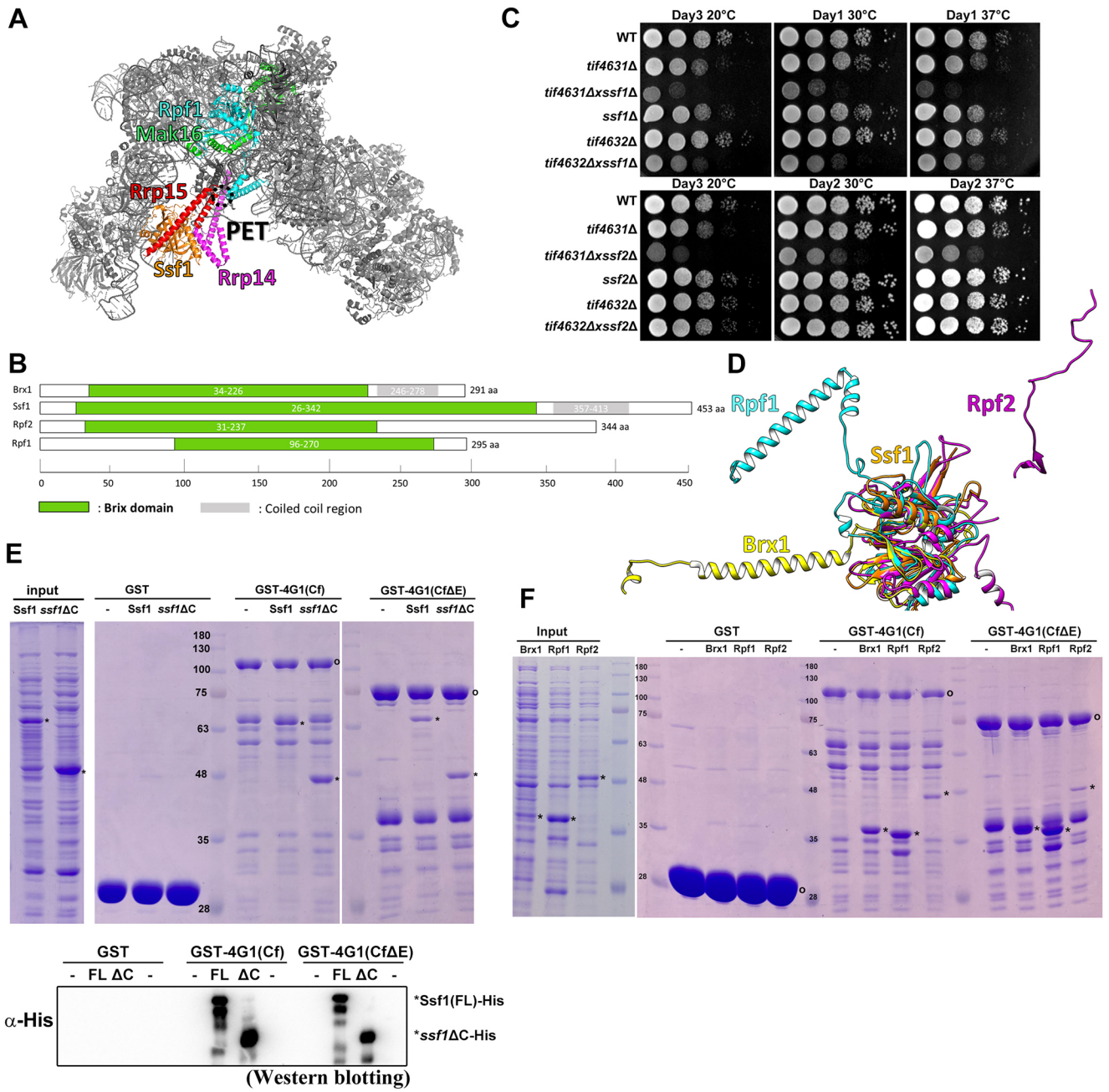

Fig. 4. *TIF4631* showed genetic and physical interaction with *SSF1*. (A) Ssf1 (orange), Rrp15 (red), Rrp14 (magenta), Rpf1 (cyan), Mak16 (green) and PET (dashed circle) are shown on the pre-60S (gray) subunit (PDB 6C0F). (B) The Brix domain (green) of each Brix family protein is shown in the diagram. (C) Growth tests of the indicated cells at different temperatures. (D) Comparisons of the structures of Ssf1, Brx1, Rpf1, and Rpf2 as revealed by Chimera (Pettersen et al., 2004) (Ssf1, Brx1, and Rpf1 protein structures were retrieved from PDB 6C0F, and Rpf2 was retrieved from PDB 3JCT). (E,F) Recombinant eIF4G1 was overexpressed in *E. coli* with a GST tag. Recombinant Ssf1, Brx1, Rpf1, or Rpf2 protein was overexpressed with His6 tags. (E) The interactions between eIF4G1 and Ssf1 were examined by Coomassie Blue staining. The interaction signals of Ssf1 and ssf1ΔC were examined by western blotting with an anti-His-tag antibody. eIF4G1 is labeled with a circle, and Ssf1 is indicated with an asterisk. FL, full length. (F) The interactions between eIF4G1 and Rpf1, Rpf2 and Brx1 were examined *in vitro*. eIF4G1 is labeled with a circle. Brx1, Rpf1 or Rpf2 is indicated with an asterisk. Images in C, E and F are representative of two experiments.

*tif4632*Δ cells (Fig. 5B); however, there were no apparent changes in Brx1, Rpf1 or Rpf2 localization (Fig. S4A–C). This is consistent with the mass spectrometry data, since the changes in these proteins were less dramatic (Fig. 3C).

Since Ssf1 and its associated protein, Rrp15, are important factors in the assembly of the PET domain (Sanghai et al., 2018), the abnormal retention of these factors might affect PET formation. The mass spectrometry data showed that the amount of Arx1 was decreased in Rlp7-containing complexes (Fig. 3C). Arx1 is a ribosome biogenesis factor that binds in the vicinity of the exit tunnel of the large subunit (Bradatsch et al., 2012; Greber et al., 2012; Hung and Johnson, 2006). Its structure is similar to methionine aminopeptidases, which catalyze the co-translational removal of N-terminal methionine from nascent polypeptides (Chang et al., 1990; Li and Chang, 1995). From the cryo-EM structure of the pre-60S complex, Arx1 binds close to the Ssf1 and Rpf1 binding sites [Fig. 5C, left panel, Nsa1-containing complex (PDB 6C0F); right panel, Nog2-containing complex (PDB 3JCT);

Journal of Cell Science (2022) 135, jcs259540. doi:10.1242/jcs.259540

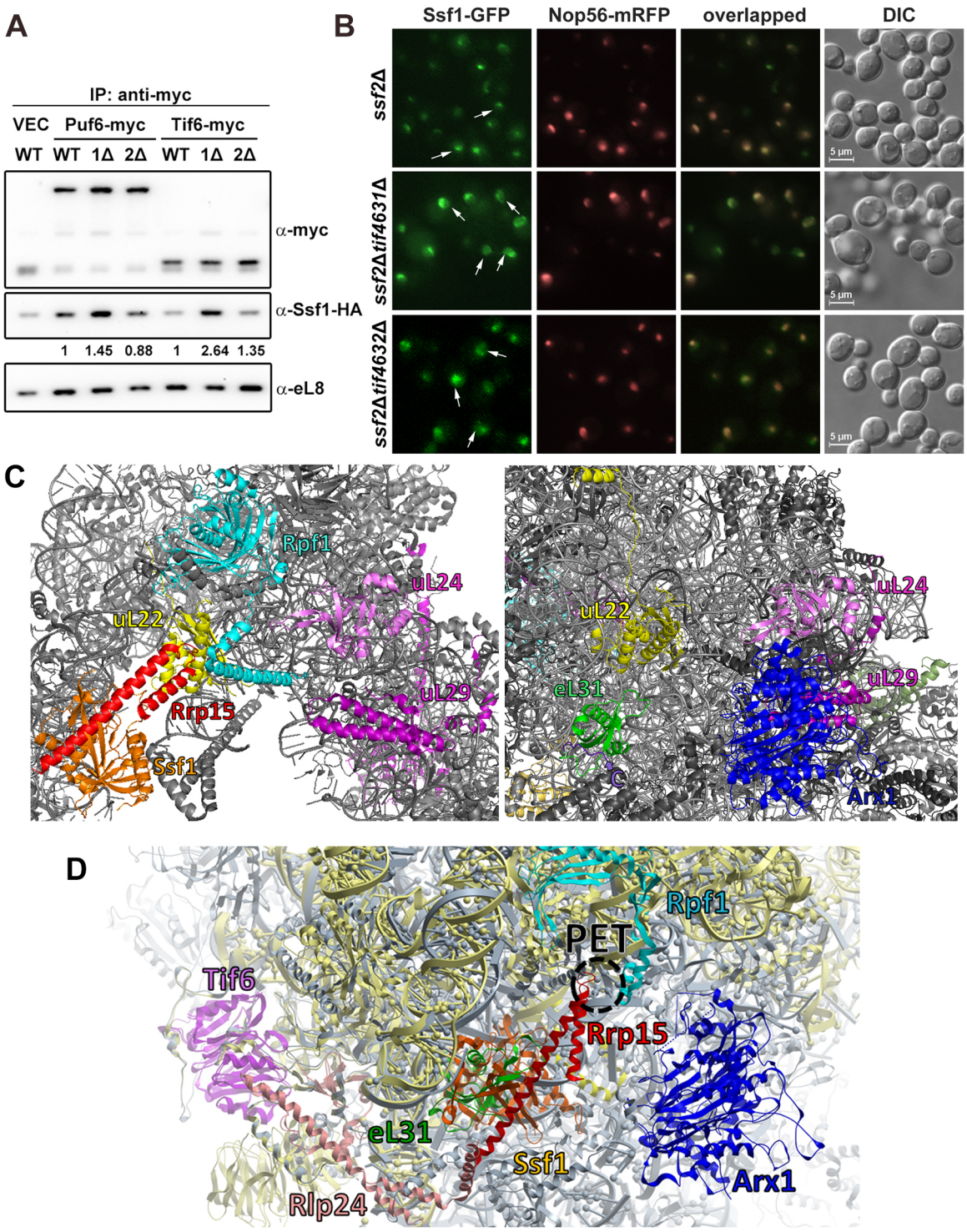

Fig. 5. Mutation of eIF4G1 caused Ssf1 retention on the pre-60S subunits. (A) The levels of Ssf1 were examined on Puf6- and Tif6-immunoprecipitated (IP) pre-60S subunits in WT, *tif4631*Δ (Δ1) or *tif4632*Δ (Δ2) cells. Values underneath the blots are the quantifications of Ssf1 levels relative to WT for the blot shown. VEC, vector only. (B) The Ssf1 localization was tracked in WT, *tif4631*Δ, and *tif4632*Δ at 30°C. Nop56–mRFP was used as the nucleolar marker. Arrows highlight the positions of the nucleolus and diffusion signals to the nucleoplasm. Images in A and B are representative of two experiments. (C) The comparisons of the PET regions of pre-60S subunits at the nucleolar stage (left panel, PDB 6C0F) or nuclear stage (right panel, PDB 3JCT). (D) Superposition of two complexes using Rlp24 as the reference by the ICM method. A close view of the PET region is shown.

Fig. 5D, superposition of two complexes by the ICM method (Abagyan and Totrov, 1994; Abagyan et al., 1994)]. In addition, it has been shown that the release of the Ssf1–Rrp15 heterodimer is a prerequisite for the loading of eL31 (Sanghai et al., 2018) (Fig. 5D). The abnormal retention of Ssf1, Rrp15 and Rrp14 might impair the proper loading of eL31 and Arx1. To test this hypothesis, we first examined the loading of Arx1 and eL31 onto the 60S ribosome. Consistent with the hypothesis, our results showed that the loading of Arx1 was significantly decreased in *tif4631*Δ cells (Fig. 6A). The loading of eL31 was also examined in WT and *tif4631*Δ cells;

Journal of Cell Science (2022) 135, jcs259540. doi:10.1242/jcs.259540

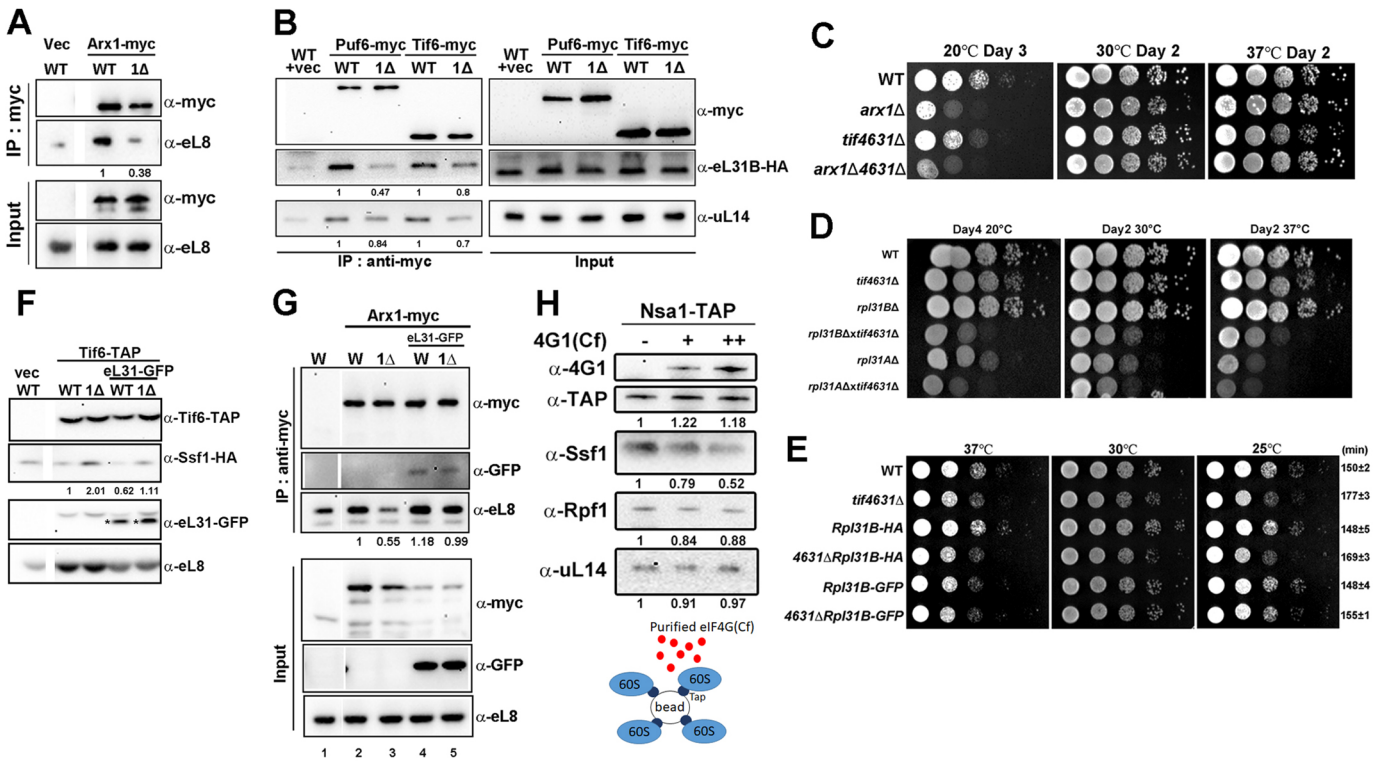

Fig. 6. Retention of Ssf1 blocks the loading of Arx1 and eL31. (A) Arx1–Myc was immunoprecipitated (IP) from WT and *tif4631*Δ (Δ1) cells. VEC, vector only. (B) The levels of eL31B and uL14 were examined on Puf6- and Tif6-immunoprecipitated pre-60S subunits in WT and *tif4631*Δ cells. (C–E) Growth tests of various strains at different temperatures. The doubling time at 25°C of each strain is shown (mean±s.d., *n*=2). Images are representative of two biological replicates. (F,G) Tif6–TAP or Arx1–Myc was immunoprecipitated from WT (W in G), *tif4631*Δ, *RPL31B-GFP* and *RPL31B-GFPtif4631*Δ cells. The position of eL31–GFP is indicated with an asterisk. (H) pre-60S was purified and immobilized on the IgG beads with Nsa1–TAP. 0 (–), 0.5 (+) and 1 (++) μg of purified eIF4G1(Cf) proteins were added and incubated for 1 h at 4°C. After several washes, the pre-60S was eluted and examined by western blotting. Images in A,B,F–H, are representative of two experiments. The quantification of the protein level normalized to WT is shown for the blots presented. 1% of lysate was used in the input blots.

compared with uL14, the eL31 decrease was more marked in nucleolar ribosomes purified through Puf6 (Fig. 6B).

The potential genetic interaction between *arx1*Δ, *rpl31*Δ and *tif4631*Δ mutants was examined (Fig. 6C,D). Notably, *arx1*Δ*tif4631*Δ showed a similar growth rate to *arx1*Δ (Fig. 6C), which supports the observations in Fig. 6A. Because Arx1 has a decreased interaction with 60S ribosomes in *tif4631*Δ cells (Fig. 6A), the double mutant was not expected to cause synthetic growth defects (Fig. 6C). eL31 has two paralogs, eL31A and eL31B, in yeast, encoded by *RPL31A* and *RPL31B*, respectively. Although the growth rate of *rpl31B*Δ cells was similar to that of WT cells, *rpl31A*Δ cells showed a slower growth rate. Once *rpl31A*Δ or *rpl31B*Δ was crossed with *tif4631*Δ, synthetic growth defects were observed in both strains (Fig. 6D). eL31 is an important protein. Although *rpl31A*Δ *rpl31b*Δ is viable, its growth is very poor (Peisker et al., 2008). Once its loading was impaired in *tif4631*Δ cells (Fig. 6B), further deletion of either paralog caused insufficiency of this ribosomal protein, resulting in worse growth (Fig. 6D).

If *tif4631*Δ disturbed the loading of eL31, overexpression of eL31 might enhance the growth rate. However, the overexpression of eL31 did not change the growth rate of *tif4631*Δ cells (Fig. S4D). Surprisingly, *RPL31B*-GFP slightly rescued the growth defect of *tif4631*Δ cells (Fig. 6E). The C-terminus of eL31 protrudes out from the pre-60S ribosomal complex (Fig. 5C, right, the C-terminus of eL31 is labeled with purple); therefore, this tag might not affect the incorporation of eL31 into 60S but rather alter the factors binding near this region. To test this assumption, Tif6- and Arx1-containing pre-60S subunits were immunoprecipitated and analyzed (Fig. 6F,G). eL31–GFP could be detected on the pre-60S subunits. The presence of eL31–GFP decreased the loading of Ssf1 (Fig. 6F) and recovered the 60S association of Arx1 (Fig. 6G, anti-eL8 signals in lane 5). Thus, Rpl31–GFP destabilized Ssf1 and facilitated the loading of Arx1 downstream.

To demonstrate whether eIF4G1 could release Ssf1, pre-60S was purified and immobilized on beads via Nsa1–TAP, and various amounts of purified eIF4G1(Cf) proteins were added. After several washes, the pre-60S complex was eluted and examined with western blotting. Although the amount of Ssf1 on pre-60S decreased with increasing amounts of eIF4G1(Cf) proteins, the Rpf1 level remained the same (Fig. 6H). In conclusion, eIF4G1 is involved in the remodeling of the PET region and the release of Ssf1. The improper release of Ssf1 in the eIF4G1 mutant impairs the downstream events of 60S biogenesis (Fig. 7).

DISCUSSION

The functional role of eIF4G1 in 60S biogenesis

In a previous study, loss of eIF4G1 was shown to cause under-accumulation of 60S ribosomal subunits (Goyer et al., 1993; Li et al., 2009). *TIF4632* is also known to be a dosage suppressor of Brix family mutants (Bogengruber et al., 2003), but the connection of eIF4G with 60S biogenesis has never been explored. This study found that eIF4G1 has a direct functional role in ribosome biogenesis. The deficiency of 60S subunits in *tif4631*Δ is not

Journal of Cell Science (2022) 135, jcs259540. doi:10.1242/jcs.259540

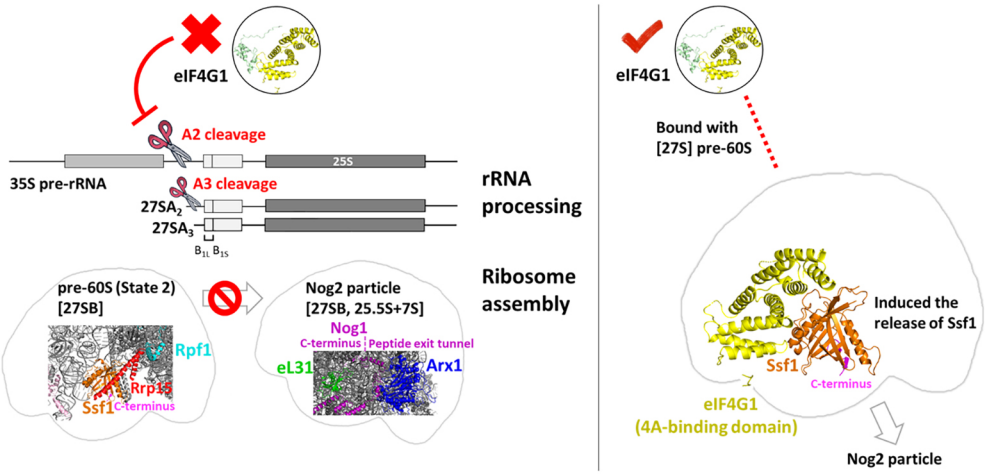

Fig. 7. Model figure. In the absence of eIF4G1, the transition to the Nog2 particle is delayed, with a high possibility of the improper release of Ssf1 and/or Rrp15, Rrp14 and Mak16. Thus, eIF4G1 is hypothesized to function in the 60S biogenesis pathway at the nucleolar stage, before Nog2 loading.

from the translational blockage, because *tif1*Δ and *tif3*Δ mutants did not show any ribosome biogenesis defects. In addition, eIF4G1 could interact with pre-60S directly.

Ssf1, Brx1 and Rpf1 pulled down higher levels of 35S rRNA in *tif4631*Δ cells, suggesting that they might improperly interact with the 90S pre-ribosome or that the cleavage of associated rRNA was not efficient. Northern blotting showed that 35S rRNA accumulated in *tif4631*Δ cells; therefore, inefficient cleavage of rRNAs is more likely. In the absence of eIF4G1, the transition to Nog2 particle was delayed, with a high possibility of the improper release of Ssf1 and/or Rrp15, Rrp14 and Mak16. Thus, eIF4G1 was hypothesized to function in the 60S biogenesis pathway at the nucleolar stage before Nog2 loading (Fig. 7).

In our study, both *tif4631*Δ and *tif4632*Δ cells showed defects in ribosome synthesis, with *tif4632*Δ having mild defects. To check whether this was caused by protein levels, *TIF4632* was expressed on a high-copy number (2 µ) plasmid to check its complementation to *tif4631*Δ. Overexpression of *TIF4632* could partially restore the growth defects and 60S deficiency of *tif4631*Δ cells but could not restore the WT level (Fig. S5). Thus, eIF4G2 might also have a role in ribosome synthesis as does eIF4G1. Further study will be required to dissect the potential functional differences between these two homologs.

eIF4G1 interacted directly with Ssf1, Brx1, Rpf1, and Rpf2, and *tif4631*Δ showed strong synthetic growth defects upon combination with *ssf1*Δ and *ssf2*Δ and slight synthetic growth defects with the conditionally depleted strains *tet-BRX1*, *GAL::RPF1* and *GAL::RPF2*. In addition, the accumulation of Ssf1 was highest in *tif4631*Δ cells compared to other Brix family proteins. One possibility is that the Brix domain of each protein interacts with pre-60S at a different orientation; thereby, the interaction surfaces of Brx1, Rpf1, and Rpf2 might not be available for eIF4G1. The binding partners of Brix proteins might also change the potential interaction with eIF4G1. Moreover, the rRNAs or proteins surrounding each Brix protein might also contribute to the interaction with eIF4G1. We cannot exclude the possibility that eIF4G1 binds at another region and triggers the release of Ssf1 indirectly. The purified eIF4G1 could only release Ssf1 but not Rpf1 from the Nsa1-containing pre-60S *in vitro*. Thus, Ssf1 is potentially the primary target of eIF4G1.

Although we could detect eIF4G1 in the 60S complex via immunoprecipitation, eIF4G1 has not been resolved with the pre-60S complex via cryo-EM. It is possible that this association is not stable. In addition, the function of eIF4G1 in 60S biogenesis has never been assigned before, and only the structures of the individual eIF4G1 domains have been elucidated (Gross et al., 2003; Grüner et al., 2016; Schütz et al., 2008). Therefore, it is difficult to assign this protein in previous cryo-EM studies. Further study is required to elucidate the specific binding site(s) of eIF4G1 on pre-60S.

Retention of Ssf1 blocks the proper loading of Arx1 and eL31

Ssf1, Rpf1 and Brx1 are typically loaded at similar stages in ribosome biogenesis, and are all required for the correct assembly of the PET domain. In *tif4631*Δ, improper retention of Ssf1 and the factors around (i.e. Rrp15, Rrp14 and Mak16), blocked the transition to state E. Thus, many factors (i.e. Arx1, Nop53, Rsa4, Nog2, and Bud20) that should be loaded downstream were present at decreased levels on the pre-60S ribosome (Fig. 7). Bud20, Rsa4, Nop53 and Arx1 levels were significantly decreased in the Rlp7-containing pre-60S complex. After Erb1 and Ytm1 are released by Mdn1, Nop53 is loaded, and Nop16 and Has1 are released from the pre-60S complex (Sanghai et al., 2018). Ssf1 and Rrp15 are also released at about the same stage, and eL31 is loaded. After these steps, Arx1 is loaded in the vicinity of the PET (Sanghai et al., 2018) (Fig. 7). Notably, eL31–GFP could partially rescue the growth of *tif4631*Δ cells and the improper loading of Arx1. The GFP tag at eL31 was found to destabilize the binding of Ssf1. Destabilization of this incorrectly retained factor on the pre-60S complex restored the downstream loading of Arx1. This data also supports the hypothesis that the retention of Ssf1 was one of the significant defects in *tif4631*Δ.

eIF4G1 has dual roles in the protein synthesis and ribosome synthesis pathways

Many critical biological pathways mutually influence each other. A growing number of studies have identified non-translational functions for many translational components, including ribosomal proteins (Lu et al., 2015; Warner and McIntosh, 2009), translation factors (Valášek et al., 2001a) and aminoacyl-tRNA synthetases (Smirnova et al., 2012). They might serve as a link to the regulation of gene expression, coordination of protein homeostasis, and other physiological pathways.

This study shows that eIF4G1 is involved in 60S ribosome biogenesis. Other translation initiation factors have also been shown to involve in ribosome biogenesis. The processing of 20S pre-rRNA to 18S rRNA happens in the cytoplasm. For this final step in the maturation of 40S ribosomal subunits, a translation-like cycle is performed (Lebaron et al., 2012; Strunk et al., 2012). The translation initiation factor eIF5B promotes the joining of mature 60S subunits to pre-40S subunits and triggers the activity of endonuclease Nob1, resulting in the cleavage of 20S rRNA. This is an important quality

Journal of Cell Science (2022) 135, jcs259540. doi:10.1242/jcs.259540

control step to verify 60S subunit binding domain before 40S ribosome can join in translation (Lebaron et al., 2012; Strunk et al., 2012). A subunit of the translation initiation factor 3 (eIF3) complex, eIF3j, is a highly conserved protein and has been shown to have an additional function in 40S ribosome biogenesis (Valášek et al., 2001a). Although eIF3j enhances critical functions of the eIF3 in translation initiation (Valasek et al., 2001b), interestingly, eIF3j also binds to the pre-40S subunit independently of eIF3 and recruits an essential nuclease for the final maturation of 18S rRNA (Valášek et al., 2001a). The use of the initiation factors in ribosome biogenesis has many advantages. First, they can be used as placeholders to direct the folding of rRNAs and create binding pockets for future use in translation. Second, they can test-drive the pre-ribosome and ensure the quality, allowing only correctly assembled ribosomes to continue translation. Incorrectly assembled ribosomes might mediate error-prone protein synthesis and be detrimental to cells. Third, they coordinate signaling between the translation and ribosome synthesis pathways. eIF4G1 does not associate with the 60S at the translation stage. Thus, it might not function as a placeholder or be involved in test driving. The advantage of involving eIF4G1 in ribosome biogenesis might be its coordination role.

eIF4G1 is also a component of P-bodies (Brengues and Parker, 2007) and stress granules (Kedersha et al., 2002). In addition, eIF4G1 has functions in pre-mRNA splicing and nuclear mRNA degradation and surveillance. Here, we further demonstrate that eIF4G1 is important in 60S ribosome biogenesis. Therefore, eIF4G1 has been suggested as a master integrator of mRNA metabolism (Das and Das, 2016). Once eIF4G1 is sequestered to P-bodies or stress granules under stress, other pathways are concurrently stopped due to the inaccessibility of eIF4G1. Additionally, the change in eIF4G1 levels is much more dynamic than that of other translation initiation factors in response to stress (Cuesta et al., 2000). Thus, tight regulation of eIF4G1 is essential to control many physiological pathways coordinately.

MATERIALS AND METHODS

Strains, plasmids and medium

All *S. cerevisiae* strains used in this study are listed in Table S1. Unless otherwise indicated, all strains were grown at 30°C in a rich medium [yeast extract peptone (Bioman)] or synthetic dropout medium [yeast nitrogen base adding selective amino acids (Sigma)] containing 2% glucose. Plasmids used in this study are listed in Table S2. Anti-uL14, anti-eL8 (Ting et al., 2017), anti-eIF4G1, anti-Ssf1 and anti-Rpf1 antibodies were generated in our laboratory. Anti-Myc antibody was obtained from MYC 1-9E10.2 [9E10] (ATCC® CRL1729™). Anti-HA (ARG62338) and anti-TAP (CAB1001) antibodies were purchased from Arigo and Thermo, respectively. The antibodies were used in 1:5000 in western blotting. Full images for western blots are shown in Fig. S6.

For growth assays, the overnight cultures were normalized to an optical density at 600 nm (OD_{600}) of 1, and ten-fold serial dilutions were made. 5 µl of the cells were spotted on the YPD (yeast extract peptone dextrose medium) plates and cultured for 2 or 3 days at temperatures indicated in the figure.

Sucrose gradient analysis

For polysome profile assays, yeast cells were collected at OD_{600} of 0.2–0.3; 50 µg/ml of cycloheximide at final concentration was added and cells were incubated for another 15 min. Polysome lysis buffer (10 mM Tris-HCl pH 7.5, 100 mM KCl, 10 mM $MgCl_2$, 6 mM β-mercaptoethanol and 200 µg/ml cycloheximide) was used for the preparation of protein extracts. Nine A_{260} (absorbance at 260 nm) units of protein extracts were loaded onto linear 7–47% sucrose gradients and spun at 40,000 rpm in a rotor (SW40 Beckman) for 2.5 h. Gradient fractions were collected on a density gradient fraction system (Brandel), continuously measuring absorbance at 254 nm. The proteins in each fraction were precipitated with 10% trichloroacetic acid (TCA) and re-dissolved in 1× SDS sample buffer. Samples were resolved in SDS-PAGE and detected by western blotting.

For monosome profile assays, the experimental conditions were similar except for the differences described below. Yeast cells were collected with no cycloheximide treatment. Cell extracts were prepared in lysis buffer (50 mM Tris-HCl pH 7.4, 50 mM NaCl and 1 mM DTT) and fractioned through a 7–47% sucrose gradient made in the same buffer.

Microscopy

Yeast cells were cultured to the log phase at different temperatures described in the figure legends. The GFP signals were directly tracked under microscopy. For immunofluorescence, log-phase cells were fixed with 3.7% formaldehyde. After cells were permeabilized with zymolyase, cells were immobilized on the poly-lysine coated slides and blocked with bovine serum albumin (BSA). Anti-HA antibody (cat. no. ARG62338, Arigo) was diluted at 1:1000 and incubated with cells overnight at 4°C. After three washes, FITC goat-anti-mouse-IgG Ab (A11001, Invitrogen, 1:300) was incubated with cells for another 2 h. After washing three times, cells were stained with DAPI. Fluorescence was visualized on a microscope (AxioScope A1; Zeiss) fitted with a Plan Apochromat 100×1.40 NA DIC objective and a digital microscopy camera (AxioCam MRm Rev. 3) controlled with AxioVision LE module Fluorescence Lite software (Zeiss). Images were prepared using Photoshop (Adobe).

Immunoprecipitation

For immunoprecipitations, cultures were grown to an OD_{600} of ∼0.5 in a selective medium. Cells were resuspended in IP buffer (20 mM Tris-HCl pH 7.5, 50 mM NaCl, 6 mM $MgCl_2$, 10% glycerol, 1 mM PMSF, and 1 mM leupeptin), and lysed by vortexing with glass beads for 30 s with 1-min interval on ice six times. For Myc- or HA-tagged strains, anti-c-Myc or anti-HA antibody was added to normalized protein extracts and incubated for 2 h at 4°C. Protein A–agarose beads (GE Healthcare) were subsequently added and incubated for another 1 h. For TAP-tagged strains, IgG–Sepharose beads (GE Healthcare) were used. After three washes, proteins were eluted in 1× Laemmli sample buffer and detected by western blotting.

Semi-quantitative mass spectrometry analysis

Purified ribosomal complexes were separated in SDS-PAGE, and the gel slices were cut and performed in-gel digestion with trypsin. Liquid chromatography tandem mass spectrometry (LC-MS/MS) analysis was performed on an Orbitrap Fusion Lumos Tribrid quadrupole-ion trap-Orbitrap mass spectrometer (Thermo Fisher Scientific, Bremen, Germany). Peptides were separated on an Ultimate system 3000 nanoLC system (Thermo Fisher Scientific, Bremen, Germany). Peptide mixtures were loaded onto a 75 µm ID, 25 cm length C18 Acclaim PepMap NanoLC column (Thermo Fisher Scientific, San Jose, CA, USA) packed with 2 µm particles with a pore of 100 Å. Mobile phase A was 0.1% formic acid in the water, and mobile phase B was 100% acetonitrile with 0.1% formic acid. A segmented gradient in 60 min from 2% to 35% solvent B at a 300 nl/min flow rate. Mass spectrometry analysis was performed in a data-dependent mode with Full-MS (externally calibrated to a mass accuracy of <5 ppm and a resolution of 120,000 at m/z=200) followed by high-energy collision activated dissociation (HCD)-MS/MS of the most intense ions for 3 s. HCD-MS/MS (resolution of 15,000) was used to fragment multiply charged ions within a 1.4 Da isolation window at a normalized collision energy of 32 eV. AGC target at 5×10^5 and 5×10^4 was set for MS and MS/MS analysis, respectively, with previously selected ions dynamically excluded for 180 s. The maximum injection time was 50 ms. For database search, the search engine is Mascot 2.3, and the setting parameters were set as below: missed cleavage, 2; MS tolerance, 10 ppm; MS/MS tolerance, 0.02 Da; Modification, Oxidation (M), Deamidation (NQ), Carbamidomethyl (C); and false discovery rate (FDR) of <1%. Only a mascot score bigger than 30 was selected. Only the proteins identified with more than two peptides were recorded. The relative abundances were calculated between WT and mutant in three independent experiments. Data were normalized by setting the ratios of the bait proteins to one. The heatmap in Fig. 3C was drawn with RStudio, and color indicates the log2 of this relative ratio.

In vitro interactions and assays

GST, GST–Tif4631 and GST–Tif4632 were constructed in pGEX-4T3 (Merck), Ssf1–His6, Brx1, Rpf1 and Rpf2 were constructed in pET21a (Novagen). The recombinant proteins were overexpressed in *E. coli* BL21. Cells were cultured in LB medium plus antibiotics at 25°C to an OD_{600} of 0.2 and induced with IPTG for 16 h. Cells were lysed in TEN100 buffer (20 mM Tris-HCl pH 7.4, 0.1 mM EDTA and 100 mM NaCl). The proteins and beads were incubated at 4°C for 1 h and sequentially washed three times with lysis buffer and eluted. Glutathione–Sepharose beads and Ni-NTA beads were purchased from GE Healthcare and Bioman, respectively.

Northern blotting

Northern blotting was used to analyze the steady-state levels of pre-rRNAs. The total RNA was extracted with the hot-phenol method (Collart and Oliviero, 2001). Affinity purified ribosomes isolated via the TAP tag were purified with IgG beads. The associated RNA was extracted with TriZol, and the RNA was resolved on a formaldehyde agarose gel. The RNAs were transferred to a nitrocellulose membrane. The probes were labeled with biotin (biotin 3′end labeling kit, Thermo Fisher Scientific) were hybridized with the membrane, and the signals were detected with North2South® Chemiluminescent hybridization and detection kit (Thermo). Probe sequences are listed in Table S3.

Acknowledgements

We thank Dr Arlen Johnson for sharing reagents and critical reviews of this manuscript. We thank the staff of the Human Disease Modeling Center at the First Core Labs, National Taiwan University College of Medicine, for sharing bioresources. We acknowledge the mass spectrometry technical research services from NTU Consortia of Key Technologies and NTU Instrumentation Center.

Competing interests

The authors declare no competing or financial interests.

Author contributions

Conceptualization: Y.-T.T., Y.-C.S., C.-Y.L., K.-Y.L.; Investigation: Y.-T.T., Y.-C.S., C.-Y.L.; Writing - original draft: Y.-T.T., K.-Y.L.; Writing – review and editing: K.-Y.L.; Supervision: K.-Y.L.; Project administration: Y.-T.T., K.-Y.L.; Funding acquisition: K.-Y.L.

Funding

This work is financially supported by the Ministry of Science and Technology, Taiwan under Contract No. MOST 106-2313-B-002-031-MY3, MOST 109-2313-B-002-023-MY3, and National Taiwan University Career Development Project (108-110L7862).

Data availability

The mass spectrometry proteomics data have been deposited to the ProteomeXchange Consortium via the PRIDE partner repository with the dataset identifier PXD033082.

Peer review history

The peer review history is available online at https://journals.biologists.com/jcs/article-lookup/doi/10.1242/jcs.259540.

References

Abagyan, R. and Totrov, M. (1994). Biased probability Monte-Carlo conformational searches and electrostatic calculations for peptides and proteins. *J. Mol. Biol.* **235**, 983-1002. doi:10.1006/jmbi.1994.1052

Abagyan, R., Totrov, M. and Kuznetsov, D. (1994). ICM – A new method for protein modeling and design - applications to docking and structure prediction from the distorted native conformation. *J. Comput. Chem.* **15**, 488-506. doi:10.1002/jcc.540150503

Altmann, M., Schmitz, N., Berset, C. and Trachsel, H. (1997). A novel inhibitor of cap-dependent translation initiation in yeast: P20 competes with eIF4G for binding to eIF4E. *EMBO J.* **16**, 1114-1121. doi:10.1093/emboj/16.5.1114

Asano, N., Kato, K., Nakamura, A., Komoda, K., Tanaka, I. and Yao, M. (2015). Structural and functional analysis of the Rpf2-Rrs1 complex in ribosome biogenesis. *Nucleic Acids Res.* **43**, 4746-4757. doi:10.1093/nar/gkv305

Ban, N., Beckmann, R., Cate, J. H. D., Dinman, J. D., Dragon, F., Ellis, S. R., Lafontaine, D. L. J., Lindahl, L., Liljas, A., Lipton, J. M. et al. (2014). A new system for naming ribosomal proteins. *Curr. Opin. Struct. Biol.* **24**, 165-169. doi:10.1016/j.sbi.2014.01.002

Baßler, J. and Hurt, E. (2019). Eukaryotic ribosome assembly. *Annu. Rev. Biochem.* **88**, 281-306. doi:10.1146/annurev-biochem-013118-110817

Baßler, J., Klein, I., Schmidt, C., Kallas, M., Thomson, E., Wagner, M. A., Bradatsch, B., Rechberger, G., Strohmaier, H., Hurt, E. et al. (2012). The conserved Bud20 zinc finger protein is a new component of the ribosomal 60S subunit export machinery. *Mol. Cell. Biol.* **32**, 4898-4912. doi:10.1128/MCB.00910-12

Bogengruber, E., Briza, P., Doppler, E., Wimmer, H., Koller, L., Fasiolo, F., Senger, B., Hegemann, J. H. and Breitenbach, M. (2003). Functional analysis in yeast of the Brix protein superfamily involved in the biogenesis of ribosomes. *FEMS Yeast Res.* **3**, 35-43. doi:10.1016/S1567-1356(02)00193-9

Bradatsch, B., Katahira, J., Kowalinski, E., Bange, G., Yao, W., Sekimoto, T., Baumgartel, V., Boese, G., Bassler, J., Wild, K. et al. (2007). Arx1 functions as an unorthodox nuclear export receptor for the 60S preribosomal subunit. *Mol. Cell* **27**, 767-779. doi:10.1016/j.molcel.2007.06.034

Bradatsch, B., Leidig, C., Granneman, S., Gnadig, M., Tollervey, D., Böttcher, B., Beckmann, R. and Hurt, E. (2012). Structure of the pre-60S ribosomal subunit with nuclear export factor Arx1 bound at the exit tunnel. *Nat. Struct. Mol. Biol.* **19**, 1234-1241. doi:10.1038/nsmb.2438

Braun, C. M., Hackert, P., Schmid, C. E., Bohnsack, M. T., Bohnsack, K. E. and Perez-Fernandez, J. (2020). Pol5 is required for recycling of small subunit biogenesis factors and for formation of the peptide exit tunnel of the large ribosomal subunit. *Nucleic Acids Res.* **48**, 405-420. doi:10.1093/nar/gkz1079

Brengues, M. and Parker, R. (2007). Accumulation of polyadenylated mRNA, Pab1p, eIF4E, and eIF4G with P-bodies in Saccharomyces cerevisiae. *Mol. Biol. Cell* **18**, 2592-2602. doi:10.1091/mbc.e06-12-1149

Calviño, F. R., Kharde, S., Ori, A., Hendricks, A., Wild, K., Kressler, D., Bange, G., Hurt, E., Beck, M. and Sinning, I. (2015). Symportin 1 chaperones 5S RNP assembly during ribosome biogenesis by occupying an essential rRNA-binding site. *Nat. Commun.* **6**, 6510. doi:10.1038/ncomms7510

Chang, Y. H., Teichert, U. and Smith, J. A. (1990). Purification and characterization of a methionine aminopeptidase from saccharomyces-cerevisiae. *J. Biol. Chem.* **265**, 19892-19897. doi:10.1016/S0021-9258(17)45456-1

Clarkson, B. K., Gilbert, W. V. and Doudna, J. A. (2010). Functional overlap between eIF4G isoforms in Saccharomyces cerevisiae. *PLoS One* **5**, e9114. doi:10.1371/journal.pone.0009114

Collart, M. A. and Oliviero, S. (2001). Preparation of yeast RNA. *Curr. Protoc. Mol. Biol.* **Chapter 13**, Unit13 12. doi:10.1002/0471142727.mb1312s23

Cuesta, R., Laroia, G. and Schneider, R. J. (2000). Chaperone Hsp27 inhibits translation during heat shock by binding eIF4G and facilitating dissociation of cap-initiation complexes. *Genes Dev.* **14**, 1460-1470. doi:10.1101/gad.14.12.1460

Das, S. and Das, B. (2016). eIF4G-an integrator of mRNA metabolism? *FEMS Yeast Res.* **16**, fow087. doi:10.1093/femsyr/fow087

Das, S., Saha, U. and Das, B. (2014). Cbc2p, Upf3p and eIF4G are components of the DRN (degradation of mRNA in the Nucleus) in Saccharomyces cerevisiae. *FEMS Yeast Res.* **14**, 922-932. doi:10.1111/1567-1364.12180

Dominguez, D., Altmann, M., Benz, J., Baumann, U. and Trachsel, H. (1999). Interaction of translation initiation factor eIF4G with eIF4A in the yeast Saccharomyces cerevisiae. *J. Biol. Chem.* **274**, 26720-26726. doi:10.1074/jbc.274.38.26720

Fatica, A., Cronshaw, A. D., Dlakić, M. and Tollervey, D. (2002). Ssf1p prevents premature processing of an early pre-60S ribosomal particle. *Mol. Cell* **9**, 341-351. doi:10.1016/S1097-2765(02)00458-6

Gerhardy, S., Menet, A. M., Peña, C., Petkowski, J. J. and Panse, V. G. (2014). Assembly and nuclear export of pre-ribosomal particles in budding yeast. *Chromosoma* **123**, 327-344. doi:10.1007/s00412-014-0463-z

Gingras, A. C., Raught, B. and Sonenberg, N. (1999). eIF4 initiation factors: effectors of mRNA recruitment to ribosomes and regulators of translation. *Annu. Rev. Biochem.* **68**, 913-963. doi:10.1146/annurev.biochem.68.1.913

Goyer, C., Altmann, M., Lee, H. S., Blanc, A., Deshmukh, M., Woolford, J. L., Jr., Trachsel, H. and Sonenberg, N. (1993). TIF4631 and TIF4632: two yeast genes encoding the high-molecular-weight subunits of the cap-binding protein complex (eukaryotic initiation factor 4F) contain an RNA recognition motif-like sequence and carry out an essential function. *Mol. Cell. Biol.* **13**, 4860-4874. doi:10.1128/MCB.13.8.4860

Greber, B. J., Boehringer, D., Montellese, C. and Ban, N. (2012). Cryo-EM structures of Arx1 and maturation factors Rei1 and Jjj1 bound to the 60S ribosomal subunit. *Nat. Struct. Mol. Biol.* **19**, 1228-1233. doi:10.1038/nsmb.2425

Gross, J. D., Moerke, N. J., von der Haar, T., Lugovskoy, A. A., Sachs, A. B., McCarthy, J. E. G. and Wagner, G. (2003). Ribosome loading onto the mRNA cap is driven by conformational coupling between eIF4G and eIF4E. *Cell* **115**, 739-750. doi:10.1016/S0092-8674(03)00975-9

Grüner, S., Peter, D., Weber, R., Wohlbold, L., Chung, M. Y., Weichenrieder, O., Valkov, E., Igreja, C. and Izaurralde, E. (2016). The structures of eIF4E-eIF4G complexes reveal an extended interface to regulate translation initiation. *Mol. Cell* **64**, 467-479. doi:10.1016/j.molcel.2016.09.020

Hentze, M. W. (1997). eIF4G– a multipurpose ribosome adapter? *Science* **275**, 500-501. doi:10.1126/science.275.5299.500

Hershey, J. W. B., Sonenberg, N. and Mathews, M. B. (2012). Principles of translational control: an overview. *Cold Spring Harbor Perspect. Biol.* **4**, a011528. doi:10.1101/cshperspect.a011528
Hung, N. J. and Johnson, A. W. (2006). Nuclear recycling of the pre-60S ribosomal subunit-associated factor Arx1 depends on Rei1 in Saccharomyces cerevisiae. *Mol. Cell. Biol.* **26**, 3718-3727. doi:10.1128/MCB.26.10.3718-3727.2006
Hung, N.-J., Lo, K.-Y., Patel, S. S., Helmke, K. and Johnson, A. W. (2008). Arx1 is a nuclear export receptor for the 60S ribosomal subunit in yeast. *Mol. Biol. Cell* **19**, 735-744. doi:10.1091/mbc.e07-09-0968
Jackson, R. J., Hellen, C. U. and Pestova, T. V. (2010). The mechanism of eukaryotic translation initiation and principles of its regulation. *Nat. Rev. Mol. Cell Biol.* **11**, 113-127. doi:10.1038/nrm2838
Kafasla, P., Barrass, J. D., Thompson, E., Fromont-Racine, M., Jacquier, A., Beggs, J. D. and Lewis, J. (2009). Interaction of yeast eIF4G with spliceosome components: implications in pre-mRNA processing events. *RNA Biol.* **6**, 563-574. doi:10.4161/rna.6.5.9861
Kaser, A., Bogengruber, E., Hallegger, M., Doppler, E., Lepperdinger, G., Jantsch, M., Breitenbach, M. and Kreil, G. (2001). Brix from Xenopus laevis and Brx1p from yeast define a new family of proteins involved in the biogenesis of large ribosomal subunits. *Biol. Chem.* **382**, 1637-1647. doi:10.1515/BC.2001.199
Kater, L., Thoms, M., Barrio-Garcia, C., Cheng, J. D., Ismail, S., Ahmed, Y. L., Bange, G., Kressler, D., Berninghausen, O., Sinning, I. et al. (2017). Visualizing the assembly pathway of nucleolar pre-60S ribosomes. *Cell* **171**, 1599-1610.e14. doi:10.1016/j.cell.2017.11.039
Kedersha, N., Chen, S., Gilks, N., Li, W., Miller, I. J., Stahl, J. and Anderson, P. (2002). Evidence that ternary complex (eIF2-GTP-tRNA(i)(Met))-deficient preinitiation complexes are core constituents of mammalian stress granules. *Mol. Biol. Cell* **13**, 195-210. doi:10.1091/mbc.01-05-0221
Kharde, S., Calviño, F. R., Gumiero, A., Wild, K. and Sinning, I. (2015). The structure of Rpf2-Rrs1 explains its role in ribosome biogenesis. *Nucleic Acids Res.* **43**, 7083-7095. doi:10.1093/nar/gkv640
Klinge, S. and Woolford, J. L. (2019). Ribosome assembly coming into focus. *Nat. Rev. Mol. Cell Biol.* **20**, 116-131. doi:10.1038/s41580-018-0078-y
Konikkat, S. and Woolford, J. L.Jr. (2017). Principles of 60S ribosomal subunit assembly emerging from recent studies in yeast. *Biochem. J.* **474**, 195-214. doi:10.1042/BCJ20160516
Kressler, D., Hurt, E. and Baßler, J. (2017). A puzzle of life: crafting ribosomal subunits. *Trends Biochem. Sci.* **42**, 640-654. doi:10.1016/j.tibs.2017.05.005
Kumar, A. (2013). CFSSP: Chou and Fasman secondary structure prediction server. *Wide Spectrum Res. J.* **1**, 15-19.
Lebaron, S., Schneider, C., van Nues, R. W., Swiatkowska, A., Walsh, D., Böttcher, B., Granneman, S., Watkins, N. J. and Tollervey, D. (2012). Proofreading of pre-40S ribosome maturation by a translation initiation factor and 60S subunits. *Nat. Struct. Mol. Biol.* **19**, 744-753. doi:10.1038/nsmb.2308
Lee, S. J. and Baserga, S. J. (1999). Imp3p and Imp4p, two specific components of the U3 small nucleolar ribonucleoprotein that are essential for pre-18S rRNA processing. *Mol. Cell. Biol.* **19**, 5441-5452. doi:10.1128/MCB.19.8.5441
Li, X. and Chang, Y. H. (1995). Amino-terminal protein processing in Saccharomyces cerevisiae is an essential function that requires two distinct methionine aminopeptidases. *Proc. Natl. Acad. Sci. USA* **92**, 12357-12361. doi:10.1073/pnas.92.26.12357
Li, Z., Lee, I., Moradi, E., Hung, N. J., Johnson, A. W. and Marcotte, E. M. (2009). Rational extension of the ribosome biogenesis pathway using network-guided genetics. *PLoS Biol.* **7**, e1000213. doi:10.1371/journal.pbio.1000213
Lo, K.-Y., Li, Z., Bussiere, C., Bresson, S., Marcotte, E. M. and Johnson, A. W. (2010). Defining the pathway of cytoplasmic maturation of the 60S ribosomal subunit. *Mol. Cell* **39**, 196-208. doi:10.1016/j.molcel.2010.06.018
Lu, H., Zhu, Y. F., Xiong, J., Wang, R. and Jia, Z. (2015). Potential extra-ribosomal functions of ribosomal proteins in Saccharomyces cerevisiae. *Microbiol. Res.* **177**, 28-33. doi:10.1016/j.micres.2015.05.004
Madru, C., Lebaron, S., Blaud, M., Delbos, L., Pipoli, J., Pasmant, E., Réty, S. and Leulliot, N. (2015). Chaperoning 5S RNA assembly. *Genes Dev.* **29**, 1432-1446. doi:10.1101/gad.260349.115
McKendrick, L., Thompson, E., Ferreira, J., Morley, S. J. and Lewis, J. D. (2001). Interaction of eukaryotic translation initiation factor 4G with the nuclear cap-binding complex provides a link between nuclear and cytoplasmic functions of the m(7) guanosine cap. *Mol. Cell. Biol.* **21**, 3632-3641. doi:10.1128/MCB.21.11.3632-3641.2001
Panse, V. G. and Johnson, A. W. (2010). Maturation of eukaryotic ribosomes: acquisition of functionality. *Trends Biochem. Sci.* **35**, 260-266. doi:10.1016/j.tibs.2010.01.001
Peisker, K., Braun, D., Wölfle, T., Hentschel, J., Fünfschilling, U., Fischer, G., Sickmann, A. and Rospert, S. (2008). Ribosome-associated complex binds to ribosomes in close proximity of Rpl31 at the exit of the polypeptide tunnel in yeast. *Mol. Biol. Cell.* **19**, 5279-5288. doi:10.1091/mbc.e08-06-0661
Peña, C., Hurt, E. and Panse, V. G. (2017). Eukaryotic ribosome assembly, transport and quality control. *Nat. Struct. Mol. Biol.* **24**, 689-699. doi:10.1038/nsmb.3454
Pettersen, E. F., Goddard, T. D., Huang, C. C., Couch, G. S., Greenblatt, D. M., Meng, E. C. and Ferrin, T. E. (2004). UCSF Chimera - a visualization system for exploratory research and analysis. *J. Comput. Chem.* **25**, 1605-1612. doi:10.1002/jcc.20084
Qiu, C., McCann, K. L., Wine, R. N., Baserga, S. J. and Hall, T. M. T. (2014). A divergent Pumilio repeat protein family for pre-rRNA processing and mRNA localization. *Proc. Natl. Acad. Sci. USA* **111**, 18554-18559. doi:10.1073/pnas.1407634112
Sanghai, Z. A., Miller, L., Molloy, K. R., Barandun, J., Hunziker, M., Chaker-Margot, M., Wang, J., Chait, B. T. and Klinge, S. (2018). Modular assembly of the nucleolar pre-60S ribosomal subunit. *Nature* **556**, 126-129. doi:10.1038/nature26156
Schuller, J. M., Falk, S., Fromm, L., Hurt, E. and Conti, E. (2018). Structure of the nuclear exosome captured on a maturing preribosome. *Science* **360**, 219-222. doi:10.1126/science.aar5428
Schütz, P., Bumann, M., Oberholzer, A. E., Bieniossek, C., Trachsel, H., Altmann, M. and Baumann, U. (2008). Crystal structure of the yeast eIF4A-eIF4G complex: an RNA-helicase controlled by protein-protein interactions. *Proc. Natl. Acad. Sci. USA* **105**, 9564-9569. doi:10.1073/pnas.0800418105
Smirnova, E. V., Lakunina, V. A., Tarassov, I., Krasheninnikov, I. A. and Kamenski, P. A. (2012). Noncanonical functions of aminoacyl-tRNA synthetases. *Biochemistry* **77**, 15-25. doi:10.1134/S0006297912010026
Sonenberg, N. and Hinnebusch, A. G. (2007). New modes of translational control in development, behavior, and disease. *Mol. Cell* **28**, 721-729. doi:10.1016/j.molcel.2007.11.018
Sonenberg, N. and Hinnebusch, A. G. (2009). Regulation of translation initiation in eukaryotes: mechanisms and biological targets. *Cell* **136**, 731-745. doi:10.1016/j.cell.2009.01.042
Strunk, B. S., Novak, M. N., Young, C. L. and Karbstein, K. (2012). A translation-like cycle is a quality control checkpoint for maturing 40S ribosome subunits. *Cell* **150**, 111-121. doi:10.1016/j.cell.2012.04.044
Sun, Q., Zhu, X., Qu, J., An, W. D., Lan, P. F., Tan, D., Chen, R. C., Wang, B., Zheng, S. D., Zhang, C. et al. (2017). Molecular architecture of the 90S small subunit pre-ribosome. *Elife* **6**, e22086. doi:10.7554/eLife.22086
Talkish, J., Zhang, J., Jakovljevic, J., Horsey, E. W. and Woolford, J. L.Jr. (2012). Hierarchical recruitment into nascent ribosomes of assembly factors required for 27SB pre-rRNA processing in Saccharomyces cerevisiae. *Nucleic Acids Res.* **40**, 8646-8661. doi:10.1093/nar/gks609
Tarun, S. Z., Jr. and Sachs, A. B. (1996). Association of the yeast poly(A) tail binding protein with translation initiation factor eIF-4G. *EMBO J.* **15**, 7168-7177. doi:10.1002/j.1460-2075.1996.tb01108.x
Ting, Y.-H., Lu, T.-J., Johnson, A. W., Shie, J.-T., Chen, B.-R., Kumar, S. S. and Lo, K.-Y. (2017). Bcp1 is the nuclear chaperone of the 60S ribosomal protein Rpl23 in Saccharomyces cerevisiae. *J. Biol. Chem.* **292**, 585-596. doi:10.1074/jbc.M116.747634
Valášek, L., Hašek, J., Nielsen, K. H. and Hinnebusch, A. G. (2001a). Dual function of eIF3j/Hcr1p in processing 20 S pre-rRNA and translation initiation. *J. Biol. Chem.* **276**, 43351-43360. doi:10.1074/jbc.M106887200
Valasek, L., Phan, L., Schoenfeld, L. W., Valaskova, V. and Hinnebusch, A. G. (2001b). Related eIF3 subunits TIF32 and HCR1 interact with an RNA recognition motif in PRT1 required for eIF3 integrity and ribosome binding. *EMBO J.* **20**, 891-904. doi:10.1093/emboj/20.4.891
Wang, W., Nag, S., Zhang, X., Wang, M. H., Wang, H., Zhou, J. W. and Zhang, R. W. (2015). Ribosomal proteins and human diseases: pathogenesis, molecular mechanisms, and therapeutic implications. *Med. Res. Rev.* **35**, 225-285. doi:10.1002/med.21327
Warner, J. R. and McIntosh, K. B. (2009). How common are extraribosomal functions of ribosomal proteins? *Mol. Cell* **34**, 3-11. doi:10.1016/j.molcel.2009.03.006
Wehner, K. A. and Baserga, S. J. (2002). The sigma(70)-like motif: a eukaryotic RNA binding domain unique to a superfamily of proteins required for ribosome biogenesis. *Mol. Cell* **9**, 329-339. doi:10.1016/S1097-2765(02)00438-0
Weis, B. L., Kovacevic, J., Missbach, S. and Schleiff, E. (2015). Plant-specific features of ribosome biogenesis. *Trends Plant Sci.* **20**, 729-740. doi:10.1016/j.tplants.2015.07.003
Woolford, J. L., Jr. and Baserga, S. J. (2013). Ribosome biogenesis in the yeast Saccharomyces cerevisiae. *Genetics* **195**, 643-681. doi:10.1534/genetics.113.153197
Wu, S., Tutuncuoglu, B., Yan, K. G., Brown, H., Zhang, Y. X., Tan, D., Gamalinda, M., Yuan, Y., Li, Z. F., Jakovljevic, J. et al. (2016). Diverse roles of assembly factors revealed by structures of late nuclear pre-60S ribosomes. *Nature* **534**, 133-137. doi:10.1038/nature17942
Yang, Y.-T., Ting, Y.-H., Liang, K.-J. and Lo, K.-Y. (2016). The roles of Puf6 and Loc1 in 60S biogenesis are interdependent, and both are required for efficient

accommodation of Rpl43. *J. Biol. Chem.* **291**, 19312-19323. doi:10.1074/jbc.M116.732800

Yu, Y. and Hirsch, J. P. (1995). An essential gene pair in saccharomyces cerevisiae with a potential role in mating. *DNA Cell Biol.* **14**, 411-418. doi:10.1089/dna.1995.14.411

Zhang, J. Y., Harnpicharnchai, P., Jakovljevic, J., Tang, L., Guo, Y. R., Oeffinger, M., Rout, M. P., Hiley, S. L., Hughes, T. and Woolford, J. L. (2007). Assembly factors Rpf2 and Rrs1 recruit 5S rRNA and ribosomal proteins rpL5 and rpL11 into nascent ribosomes. *Genes Dev.* **21**, 2580-2592. doi:10.1101/gad.1569307

Zhou, D. J., Zhu, X., Zheng, S. D., Tan, D., Dong, M.-Q. and Ye, K. Q. (2019). Cryo-EM structure of an early precursor of large ribosomal subunit reveals a half-assembled intermediate. *Protein Cell* **10**, 120-130. doi:10.1007/s13238-018-0526-7